Doping-dependent charge order correlations in electron-doped cuprates

Eduardo H. da Silva Neto,[1,2,3,4]* Biqiong Yu,[5] Matteo Minola,[3] Ronny Sutarto,[6] Enrico Schierle,[7] Fabio Boschini,[1,2] Marta Zonno,[1,2] Martin Bluschke,[3,7] Joshua Higgins,[8] Yangmu Li,[5] Guichuan Yu,[5] Eugen Weschke,[7] Feizhou He,[6] Mathieu Le Tacon,[3,9] Richard L. Greene,[8] Martin Greven,[5] George A. Sawatzky,[1,2] Bernhard Keimer,[3] Andrea Damascelli[1,2]*

Understanding the interplay between charge order (CO) and other phenomena (for example, pseudogap, antiferromagnetism, and superconductivity) is one of the central questions in the cuprate high-temperature superconductors. The discovery that similar forms of CO exist in both hole- and electron-doped cuprates opened a path to determine what subset of the CO phenomenology is universal to all the cuprates. We use resonant x-ray scattering to measure the CO correlations in electron-doped cuprates ($La_{2-x}Ce_xCuO_4$ and $Nd_{2-x}Ce_xCuO_4$) and their relationship to antiferromagnetism, pseudogap, and superconductivity. Detailed measurements of $Nd_{2-x}Ce_xCuO_4$ show that CO is present in the $x = 0.059$ to 0.166 range and that its doping-dependent wave vector is consistent with the separation between straight segments of the Fermi surface. The CO onset temperature is highest between $x = 0.106$ and 0.166 but decreases at lower doping levels, indicating that it is not tied to the appearance of antiferromagnetic correlations or the pseudogap. Near optimal doping, where the CO wave vector is also consistent with a previously observed phonon anomaly, measurements of the CO below and above the superconducting transition temperature, or in a magnetic field, show that the CO is insensitive to superconductivity. Overall, these findings indicate that, although verified in the electron-doped cuprates, material-dependent details determine whether the CO correlations acquire sufficient strength to compete for the ground state of the cuprates.

INTRODUCTION

In the copper oxide materials, the doping of either hole or electron carriers into the parent Mott insulator suppresses antiferromagnetism (AFM) and allows the appearance of superconductivity (1). Several studies have shown that the cuprates also feature a tendency toward a periodic self-organization of their charge degrees of freedom, known as charge order (CO) (2–14). Although CO is now accepted as a ubiquitous phenomenon in the cuprates, the situation regarding its interrelationship with AFM, superconductivity, and the pseudogap is less clear. For example, in the La-based hole cuprates, the CO periodicity increases as a function of doping and is closely related to the antiferromagnetic incommensurability near the hole-doping level 1/8 (2, 15), but this connection is absent in other cuprates (8, 9, 11, 16–18). Regarding the pseudogap, whereas x-ray and scanning tunneling microscopy (STM) measurements show the CO onsets below or at the pseudogap temperature (T^*) in hole-doped cuprates (8, 16, 17, 19), the opposite behavior is observed in electron-doped cuprates (12). Finally, several studies point toward a competition between CO and superconductivity (2, 3, 5, 6, 9, 20–23), although this has not yet been experimentally verified in electron-doped cuprates because of the lack of measurements across the superconducting transition temperature (T_c), as a function of doping, or in the presence of a magnetic field.

Despite the wealth of experimental studies of CO in the hole-doped cuprates, a comprehensive study of the electron-doped counterparts has not yet been reported. If CO is also found to be a universal property of the electron-doped cuprates, detailed knowledge of its behavior as a function of doping, temperature, and magnetic field can be used not only to determine which emergent phenomena (that is, superconductivity, pseudogap, and AFM) are truly intrinsically connected to CO formation but also to provide clues about its microscopic origin. For example, because of the robustness of antiferromagnetic correlations in electron-doped cuprates relative to the hole-doped materials, the study of the CO in the former might serve as a test of several theoretical models in which CO is magnetically driven (24–27). It has been shown that for $Nd_{2-x}Ce_xCuO_4$ (NCCO) near optimal doping, the CO wave vector (Q_{CO}) connects the areas of the Brillouin zone near where the antiferromagnetic zone boundary intercepts the underlying Fermi surface, similar to observations in Bi-based hole-doped cuprates (8, 9, 28). Further supporting this connection between CO and AFM is the observation that the temperature scales for the two phenomena approximately coincide with NCCO near optimal doping. However, the relationships between CO and AFM in momentum space and in temperature have not yet been studied as a function of doping. This comprehensive doping-temperature study of the CO should clarify its connection not only to AFM but also to the pseudogap phenomenon, which, in electron-doped cuprates, is thought to be derived from the AFM (1).

[1]Department of Physics and Astronomy, University of British Columbia, Vancouver, British Columbia V6T 1Z1, Canada. [2]Quantum Matter Institute, University of British Columbia, Vancouver, British Columbia V6T 1Z4, Canada. [3]Max Planck Institute for Solid State Research, Heisenbergstrasse 1, D-70569 Stuttgart, Germany. [4]Quantum Materials Program, Canadian Institute for Advanced Research, Toronto, Ontario M5G 1Z8, Canada. [5]School of Physics and Astronomy, University of Minnesota, Minneapolis, MN 55455, USA. [6]Canadian Light Source, Saskatoon, Saskatchewan S7N 2V3, Canada. [7]Helmholtz-Zentrum Berlin für Materialien und Energie, Albert-Einstein-Strasse 15, D-12489 Berlin, Germany. [8]Center for Nanophysics and Advanced Materials, University of Maryland, College Park, MD 20742, USA. [9]Institut für Festkörperphysik, Karlsruher Institut für Technologie, 76201 Karlsruhe, Germany.
*Corresponding author. Email: ehda@physics.ubc.ca (E.H.d.S.N.); damascelli@physics.ubc.ca (A.D.)

RESULTS

Before investigating the universality of the CO phenomenology, we initially demonstrated the presence of CO correlations in a second member of the electron-doped family, $La_{2-x}Ce_xCuO_4$ (LCCO). To reveal the CO correlations in this material, we performed resonant x-ray scattering
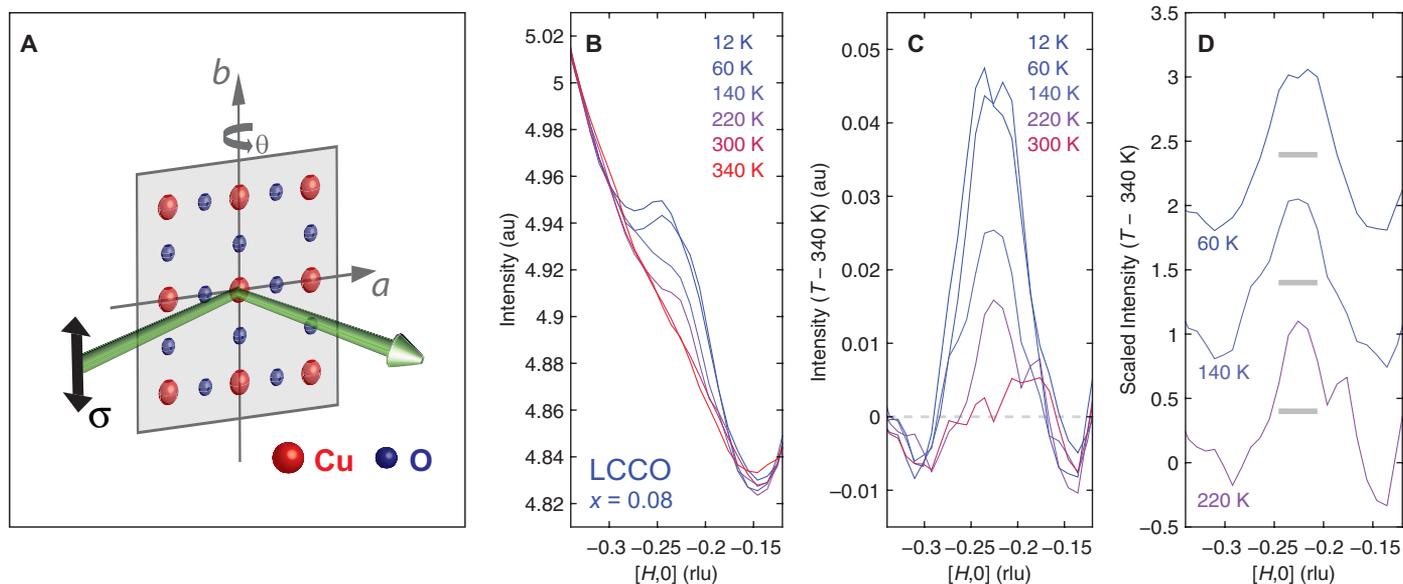
Fig. 1. CO in LCCO. (A) Scattering geometry along the Cu–O bond direction (see text for details). **(B)** RXS θ scans for LCCO ($x = 0.08$, $T_c \sim 20$ K) at various temperatures. au, arbitrary units. **(C)** CO peaks at different temperatures obtained upon subtracting the 340 K data from those at lower temperatures. **(D)** Data (60, 140, and 220 K) from (C) with their maxima normalized to unit. The curves were offset for clarity, and the width of gray bars represents the half width at half maximum of the 60 K data.

(RXS) measurements at the Cu-L_3 edge. The in-plane components of momentum transfer along the a axis were accessed by rotating the sample about the b axis (θ scan) while maintaining the scattering geometry (angles of incoming and outgoing photons) fixed, as depicted in Fig. 1A. All momentum transfer components $Q = (H, K, L)$ are reported in reciprocal lattice units (rlu). Figure 1 (B to D) shows our RXS measurements of LCCO, which were performed at various temperatures. It is clear from the θ scans in Fig. 1B that a peak near $H = -0.22$ is present at 12 K, weakens as the temperature is raised, and disappears above 220 K. The suppression of this peak either with temperature or by tuning the photon energy away from resonance (29) demonstrates the presence of CO in LCCO and validates the presence of CO in electron-doped cuprates. Unlike previous work for NCCO (12), the data in LCCO show a featureless high-temperature θ scan, which provides a good measure of the temperature-independent background. Subtraction of the 340 K data reveals a CO peak with similar width (~25 Å correlation length in real space) and intensity as for NCCO (see Fig. 1C). Furthermore, it also reveals that the peak width is remarkably temperature-independent, as can be seen more clearly in Fig. 1D, which shows the curves in Fig. 1C normalized by their maxima. As we will discuss below, the temperature independence of the CO correlation length also appears to be present in NCCO and provides a key difference between the phenomenologies of YBa$_2$Cu$_3$O$_{6+\delta}$ (YBCO), as well as La$_{2-\delta}$(Ba,Sr)$_\delta$CuO$_4$, and electron-doped cuprates.

Figure 2 (A to F) shows θ scans at a number of temperatures for six different doping levels of NCCO. It is clear from these measurements that the CO is absent for $x = 0.042$ at low temperatures. Measurements above the Néel temperature (see Fig. 2A) indicate that doping, rather than competition for the ground state, is responsible for the suppression of the CO at this doping range. Figure 2 (C to E) also explicitly shows that $Q_{CO}(x)$ increases as a function of x. In Fig. 3A, we summarize $Q_{CO}(x)$ and, from comparison to previous angle-resolved photoemission spectroscopy (ARPES) reports (30, 31), show that it connects

the parallel segments near (π,0). The value of $Q_{CO}(x)$ for $x = 0.14$ is also consistent with inelastic hard x-ray scattering measurements that detect an anomalous softening of the bond-stretching mode at $H = 0.20 \pm 0.03$ (32). Here, we observe that because of the Fermi surface topology, we cannot rule out whether $Q_{CO}(x)$ connects the inter–hot spot distance (29), although, as we show below (Fig. 3B), the combined doping-temperature dependence of the CO seems uncorrelated to T^* (12). Although this observation, together with the absence of gaps near (π,0) above T_c, suggests that Fermi surface nesting is not responsible for the CO formation, it is possible that the CO becomes neither long-range nor intense enough to modify the Fermi surface. Nevertheless, note that a similar behavior of the CO peak is observed in YBCO and Bi cuprates, where $Q_{CO}(x)$ also follows the Fermi surface (8, 9, 16). Therefore, our finding for $Q_{CO}(x)$ adds to the list of similarities between NCCO and hole-doped COs—in addition to the similar wave vector, coherence length, and RXS intensity (the last two in Bi cuprates)—and further supports a common origin for their existence.

The possible connection between $Q_{CO}(x)$ and the inter–hot spot distance suggests that perhaps antiferromagnetic fluctuations are intrinsically connected to the appearance of CO instabilities. To explore this idea, we turn to the temperature dependence of the CO for NCCO and compare it to previous inelastic neutron scattering (INS) studies that probed the instantaneous antiferromagnetic fluctuations (33). To ensure a direct experimental comparison, we used crystals that were either obtained from larger pieces used in the previous INS study (33) or synthesized by the same method (29). For $x = 0.059$, a weak CO peak is barely detectable, as shown in Fig. 2B, and completely disappears above room temperature. The relative weakness of the CO peak for this sample precludes a precise measurement of its onset temperature. Upon further doping, the $x = 0.078$ sample shows a clearer CO peak that, at $T_{CO}^O = 260 \pm 60$ K, also completely disappears. However, this behavior qualitatively changes for $x = 0.106$, where the CO peak apparently saturates at a finite value, T_{CO}^S, above room temperature, as shown in Fig. 2 (D to
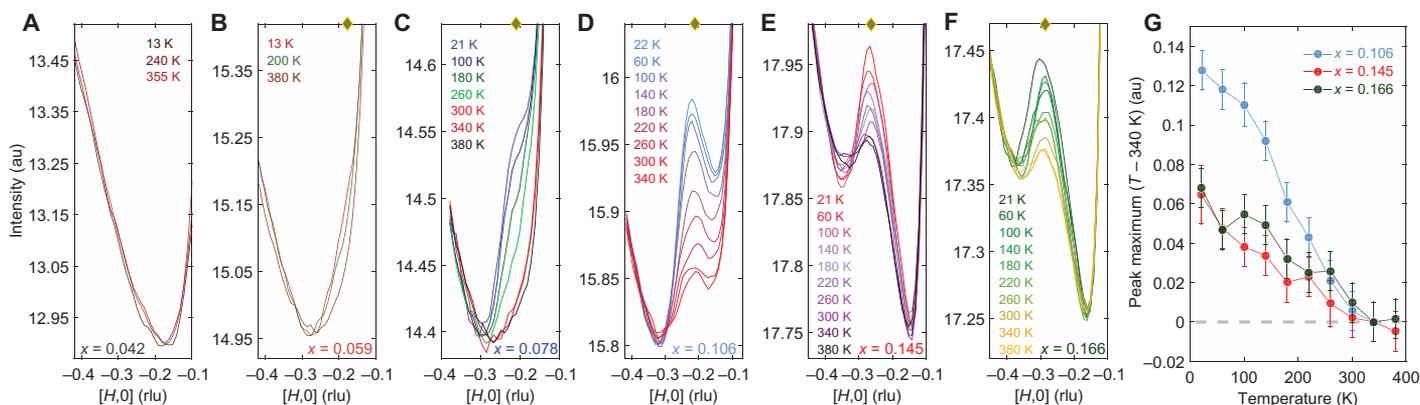
Fig. 2. Temperature and doping dependence of CO in NCCO. (**A** to **F**) Temperature dependence of θ scans for six doping levels of NCCO. Yellow diamonds in (A) to (F) show the H location of the low-temperature peak maxima (29). (**G**) Temperature dependence of the CO peak maximum after subtraction of the 340 K peak maximum (29), extracted from the data in (D) to (F). The vertical scales in (A) to (F) are proportional to the detector reading normalized to the incoming photon flux (29). Note that the intensity difference in the vertical scale of (G) is plotted in the same units as in (D) to (F). The error bars in (G) represent the systematic errors associated with the experiment (29).

F). The reason for this behavior is not clear, and we cannot distinguish whether it is truly a saturation or a change in the rate at which the CO is suppressed with temperature—the latter would require measurements at temperatures higher than what is currently technically possible. This temperature dependence is summarized in Fig. 2G, where the peak maximum (after subtracting the 340 K data) is shown for the data in Fig. 2 (D to F). Unfortunately, the high-temperature behavior, discussed above, precludes the determination of the true background and renders any determination of the CO intensity versus doping unreliable (29). Nevertheless, it is obvious that above $x = 0.042$, the CO temperature scale increases up to $x = 0.106$ and remains high (above 300 K) with further electron doping. The behavior of the characteristic temperatures shows a trend opposite to the antiferromagnetic correlations, as summarized in Fig. 3B, and suggests that the two phenomena are not intrinsically related.

For a typical second-order phase transition, the correlation length and susceptibility increase upon cooling in the disordered phase. This behavior of the CO is seen in YBCO above T_c. However, as Fig. 1 shows, the CO peak width in LCCO is temperature-independent, and the correlation length never increases above ~25 Å. At first sight, this clear assertion cannot be made about the correlation length of the CO in NCCO because the presence of a peak at all measured temperatures precludes the identification of the true background. Nevertheless, the data in Fig. 2 (D to F) show that the peak develops on top of a concave fluorescence background, displaying a distinct local minimum for H less than Q_{CO}. Under these conditions, this minimum should move away from Q_{CO} if the width increased with temperature—a behavior that is clearly not present in the data (29). Therefore, although a precise measure of the peak width as a function of temperature cannot be obtained, we can conclude that, as in LCCO, and contrary to YBCO, the correlation length in NCCO is approximately independent of temperature. This behavior, as well as the short correlation length, resembles the observations for hole-doped Bi cuprates (8, 9) and $HgBa_2CuO_{4+\delta}$ (Hg1201) (11).

Another feature of the CO in YBCO, as well as in $La_{2-\delta}Sr_\delta CuO_4$ (where the CO is short-range), is that both its correlation length and integrated intensity are suppressed below T_c—a clear indication of a competition between ordered states (5, 6, 22, 23, 34). Figure 4A shows

θ scans measured below and above T_c, showing that the CO peak is remarkably insensitive to superconductivity in NCCO. This behavior is not without precedent, because signatures of competition in the temperature dependence of other hole-doped cuprates are not clearly present in the RXS data (9, 11).

The relationship between the CO and superconductivity can also be probed by measurements in applied magnetic fields. In the case of YBCO, fields up to 18 T enhance the CO peak (6, 16, 17), and at higher fields, above the superconducting upper critical field, H_{c2}, the CO becomes long-range and three-dimensional (35–37), again indicating a competition between superconductivity and CO. Therefore, given that NCCO has a much lower H_{c2} (~10 T at 0 K) (38, 39) than hole-doped cuprates, one might expect that an even smaller magnetic field enhances the CO signal. Measurements in the presence of a magnetic field are more challenging because of field-induced mechanical distortions of the sample environment that can cause significant modifications to the background of the θ scans (29). Nevertheless, Fig. 4B shows that at 10 K, below T_c, no appreciable difference is seen in the scattering peak up to 6 T (the upper limit allowed by our instrument). This finding suggests an insensitivity of the CO to the superconducting order, consistent with both the zero-field data across T_c (Fig. 4A) and the doping dependence (Fig. 3B).

DISCUSSION

Our comprehensive data for the doping, temperature, and magnetic field dependence of the CO in NCCO and LCCO allow us to make a direct comparison to YBCO, a material for which CO has been extensively characterized over the past few years. We find that the CO in NCCO differs from the behavior of its YBCO analog in three ways: (i) it is insensitive to superconductivity; (ii) it has a small, temperature-independent correlation length; and (iii) it can be present up to very high temperatures. The YBCO experiments have been interpreted as evidence for competition between different many-electron ground states. Clearly, this description does not apply to the CO in NCCO.

We consider two possible scenarios for the interpretation of our data. First, we refer to recent theoretical work that proposes that disorder-induced
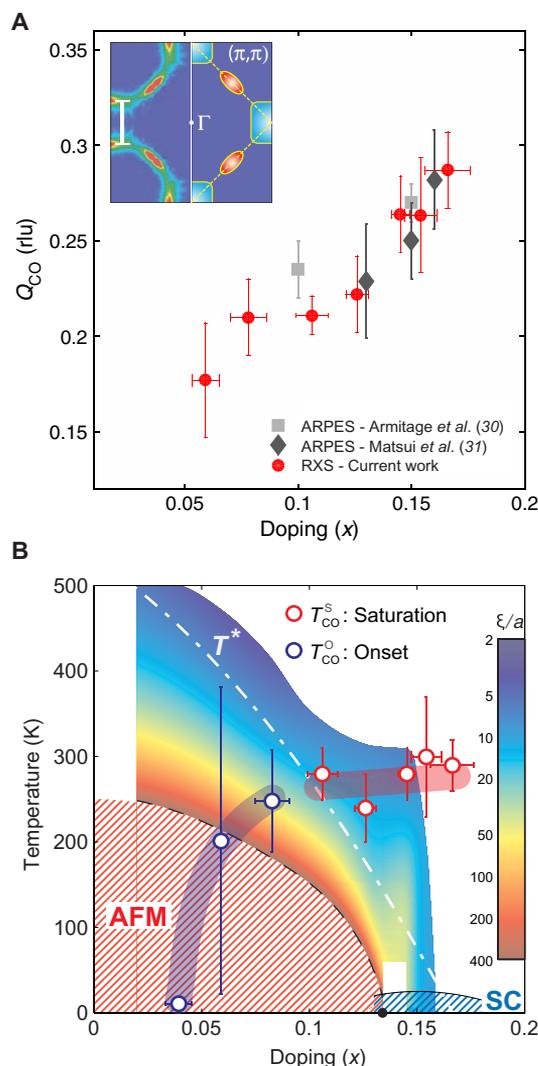
Fig. 3. Phase diagram of CO in NCCO. (**A**) Doping dependence of $Q_{CO}(x)$ compared with the separation between the segments of the Fermi surface near $(\pi,0)$, as determined from ARPES (white bar in the inset). The inset shows a representative ARPES Fermi surface NCCO for $x = 0.15$ (left) and a schematic of the AFM-folded Fermi surface (right), with electron (blue) and hole (red) pockets. (**B**) Phase diagram of NCCO adapted from the study by Motoyama *et al.* (*33*), including the AFM and superconductivity (SC) region, the pseudogap temperature (T^*), and the instantaneous antiferromagnetic correlation length (ξ) (normalized to the tetragonal lattice constant a) determined via INS. Superimposed red and blue circles represent T_{CO}^O and T_{CO}^S, respectively. Thick semitransparent blue and red lines are guides to the eye. In (A) and (B), the horizontal error bars represent the uncertainty in the experimental determination of doping level (*29*). The vertical error bars in (B) indicate the uncertainty in locating the temperature where T_{CO}^O and T_{CO}^S deviate from their respective high-temperature behaviors (*29*).

Friedel oscillations are responsible for the observation of RXS peaks, akin to quasiparticle interference modulations seen by STM (*40*, *41*). Although the short, temperature-independent correlation length observed in our measurements might be explained by the length scale of the disorder potential in this scenario, and microstructural defects that can act as potential pinning sites are present in NCCO (*42*), at this point
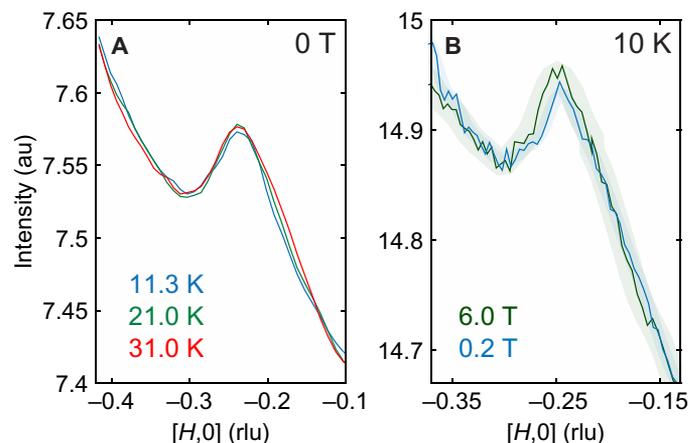
Fig. 4. CO versus superconductivity. (**A** and **B**) Measurements of an $x = 0.14$ sample ($T_c \sim 22$ K) (A) at 0 T as a function of temperature above and below T_c, and (B) at 10 K for 0.2 and 6.0 T. The halos around the curves in (B) represent the experimental uncertainty from magnetic field–induced mechanical distortions of the sample environment (*29*). Data in (A) and (B) were obtained using different instruments at the same beamline (*29*).

only detailed spatially resolved measurements could validate this scenario. As for the second scenario, we note that, in our experiments, we do not have the ability to select the energy of the scattered photons, and our measurements should be regarded as energy-integrated. Therefore, as an alternative interpretation, it is possible that the CO peaks in NCCO and LCCO, and possibly even in Bi-based cuprates and Hg1201, are a signature of CO fluctuations rather than static order, in a manner resembling thermal diffuse scattering from soft but weakly temperature-dependent lattice vibrations. Although the observed softening of the bond-stretching phonon mode (*32*) is likely related to the CO, static order is expected to induce a corresponding lattice distortion in NCCO, which has not yet been observed—unlike the case for YBCO where hard x-ray scattering also detects the CO (*6*, *17*). In this context, it is also worth mentioning that a fluctuating order competing with superconductivity has been observed in NCCO ($x = 0.156$) (*43*). Although a correspondence between this fluctuating order and the CO studied here cannot yet be concluded, we raise the possibility that the competition between superconductivity and the CO can only be observed by separating its inelastic signal from the impurity-pinned quasielastic component. At this point, only more detailed studies of the electronic excitation spectrum will be able to resolve the energy structure of the CO in electron-doped cuprates.

Clearly, the tendency for the charge degrees of freedom to self-organize is ubiquitous to hole- and electron-doped cuprates, strongly suggesting a common physical origin for these correlations. However, the realization of these CO correlations into a thermodynamic order that competes for the ground state of the system in zero field is likely material-dependent. The suppression of T_c that occurs in YBCO and LBCO near 1/8 doping is not reported in other cuprates. Factors that could influence the ground state selection include materials-specific lattice distortions, details of the Fermi surface, and disorder. Finally, our experiments also show that the CO is not directly linked to either antiferromagnetic correlations or the pseudogap in electron-doped cuprates. Overall, our findings should constrain any future endeavors aiming to provide a microscopic theory of CO formation in the cuprates.

MATERIALS AND METHODS

Crystal growth and characterization

NCCO crystals used for the temperature and doping-dependent measurements displayed in Figs. 2 and 3 were grown by the Minnesota group in an oxygen flow at a pressure of 4 atm using the traveling solvent floating zone technique. For all doping levels (except $x = 0.042$), the crystals went through an oxygen reduction process. The reduction procedure was as follows: 10 hours in Ar gas at 970°C, followed by 20 hours in O_2 at 500°C. The actual doping levels were determined either via inductively coupled plasma or by wavelength-dispersive spectroscopy (WDS) measurements. Most samples were cut from larger crystals measured in a previous INS measurement (33). NCCO crystals used for the measurements displayed in Fig. 4 were grown by the Maryland group using the flux method and annealed for 2 days at the appropriate temperature to render them superconducting (1). The Ce concentration of the crystals was determined using WDS analysis. The c-axis–oriented LCCO ($x = 0.08$) films were deposited directly on (100) $SrTiO_3$ substrates by a pulsed laser deposition technique using a KrF excimer laser as the exciting light source. The films were typically 100 to 150 nm in thickness. The samples were optimized by annealing to give a maximum T_c for the 0.08 Ce doping and a narrow transition temperature width. The T_c was typically 20 ± 1 K. As typical, the normal-state resistivity (in a field above H_{c2}) shows a low-temperature upturn. These LCCO films are similar to those prepared for other experiments by the Maryland group (44). Further details can be found in the Supplementary Materials.

Resonant x-ray scattering

Zero-field RXS measurements were performed at the REIXS (Resonant Elastic and Inelastic X-ray Scattering) beamline of the Canadian Light Source in the 20 to 380 K range and in the ultrahigh vacuum diffractometer at the UE46-PGM1 beamline of BESSY II (Berliner Elektronenspeicherring für Synchrotronstrahlung) at the Helmholtz-Zentrum Berlin, which allowed measurements down to 10 K. Magnetic field measurements were performed at the high-field diffractometer of the same beamline in BESSY II. To maximize the CO diffraction signal, all measurements were performed in σ geometry (photon polarization in the a-b plane) and with the incoming photon energy tuned to the Cu-L_3 edge (~932 eV). The θ scans were performed with the detector angle fixed at 170°, resulting in L values near 1.6 rlu at the peak positions. NCCO samples grown by the traveling floating zone technique had to be polished for the CO peak to be more clearly observed. Measurements on the polished crystals were consistent with identical measurements on the crystals grown by the flux method, with the latter naturally yielding shiny homogeneous surfaces that were appropriate for our RXS experiments.

SUPPLEMENTARY MATERIALS

Supplementary material for this article is available at http://advances.sciencemag.org/cgi/content/full/2/8/e1600782/DC1

Supplementary Materials and Methods
table S1. Summary of NCCO samples used for RXS measurements.
fig. S1. ARPES measured Fermi surface of NCCO for $x = 0.15$.
fig. S2. Comparison between CO wave vector measured by RXS and inferred by ARPES.
fig. S3. Patching of the data acquired in the high-field diffractometer chamber at BESSY II.
fig. S4. Schematic drawing of the scattering geometry in the high-field diffractometer chamber at BESSY II.
fig. S5. Energy dependence of RXS scans in LCCO.

REFERENCES AND NOTES

1. N. P. Armitage, P. Fournier, R. L. Greene, Progress and perspectives on electron-doped cuprates. Rev. Mod. Phys. 82, 2421–2487 (2010).
2. J. M. Tranquada, B. J. Sternlieb, J. D. Axe, Y. Nakamura, S. Uchida, Evidence for stripe correlations of spins and holes in copper oxide superconductors. Nature 375, 561–563 (1995).
3. P. Abbamonte, A. Rusydi, S. Smadici, G. D. Gu, G. A. Sawatzky, D. L. Feng, Spatially modulated 'Mottness' in La$_{2-x}$Ba$_x$CuO$_4$. Nat. Phys. 1, 155–158 (2005).
4. T. Wu, H. Mayaffre, S. Krämer, M. Horvatić, C. Berthier, W. N. Hardy, R. Liang, D. A. Bonn, M.-H. Julien, Magnetic-field-induced charge-stripe order in the high-temperature superconductor YBa$_2$Cu$_3$O$_y$. Nature 477, 191–194 (2011).
5. G. Ghiringhelli, M. Le Tacon, M. Minola, S. Blanco-Canosa, C. Mazzoli, N. B. Brookes, G. M. De Luca, A. Frano, D. G. Hawthorn, F. He, T. Loew, M. Moretti Sala, D. C. Peets, M. Salluzzo, E. Schierle, R. Sutarto, G. A. Sawatzky, E. Weschke, B. Keimer, L. Braicovich, Long-range incommensurate charge fluctuations in (Y,Nd)Ba$_2$Cu$_3$O$_{6+x}$. Science 337, 821–825 (2012).
6. J. Chang, E. Blackburn, A. T. Holmes, N. B. Christensen, J. Larsen, J. Mesot, R. Liang, D. A. Bonn, W. N. Hardy, A. Watenphul, M. v. Zimmermann, E. M. Forgan, S. M. Hayden, Direct observation of competition between superconductivity and charge density wave order in YBa$_2$Cu$_3$O$_{6.67}$. Nat. Phys. 8, 871–876 (2012).
7. A. J. Achkar, R. Sutarto, X. Mao, F. He, A. Frano, S. Blanco-Canosa, M. Le Tacon, G. Ghiringhelli, L. Braicovich, M. Minola, M. Moretti Sala, C. Mazzoli, R. Liang, D. A. Bonn, W. N. Hardy, B. Keimer, G. A. Sawatzky, D. G. Hawthorn, Distinct charge orders in the planes and chains of ortho-III-ordered YBa$_2$Cu$_3$O$_{6+\delta}$ superconductors identified by resonant elastic x-ray scattering. Phys. Rev. Lett. 109, 167001 (2012).
8. R. Comin, A. Frano, M. M. Yee, Y. Yoshida, H. Eisaki, E. Schierle, E. Weschke, R. Sutarto, F. He, A. Soumyanarayanan, Y. He, M. Le Tacon, I. S. Elfimov, J. E. Hoffman, G. A. Sawatzky, B. Keimer, A. Damascelli, Charge order driven by Fermi-arc instability in Bi$_2$Sr$_{2-x}$La$_x$CuO$_{6+\delta}$. Science 343, 390–392 (2014).
9. E. H. da Silva Neto, P. Aynajian, A. Frano, R. Comin, E. Schierle, E. Weschke, A. Gyenis, J. Wen, J. Schneeloch, Z. Xu, S. Ono, G. Gu, M. Le Tacon, A. Yazdani, Ubiquitous interplay between charge ordering and high-temperature superconductivity in cuprates. Science 343, 393–396 (2014).
10. M. Hashimoto, G. Ghiringhelli, W.-S. Lee, G. Dellea, A. Amorese, C. Mazzoli, K. Kummer, N. B. Brookes, B. Moritz, Y. Yoshida, H. Eisaki, Z. Hussain, T. P. Devereaux, Z.-X. Shen, L. Braicovich, Direct observation of bulk charge modulations in optimally doped Bi$_{1.5}$Pb$_{0.6}$Sr$_{1.54}$CaCu$_2$O$_{8+\delta}$. Phys. Rev. B 89, 220511(R) (2014).
11. W. Tabis, Y. Li, M. Le Tacon, L. Braicovich, A. Kreyssig, M. Minola, G. Dellea, E. Weschke, M. J. Veit, M. Ramazanoglu, A. I. Goldman, T. Schmitt, G. Ghiringhelli, N. Barišić, M. K. Chan, C. J. Dorow, G. Yu, X. Zhao, B. Keimer, M. Greven, Charge order and its connection with Fermi-liquid charge transport in a pristine high-T_c cuprate. Nat. Commun. 5, 5875 (2014).
12. E. H. da Silva Neto, R. Comin, F. He, R. Sutarto, Y. Jiang, R. L. Greene, G. A. Sawatzky, A. Damascelli, Charge ordering in the electron-doped superconductor Nd$_{2-x}$Ce$_x$CuO$_4$. Science 347, 282–285 (2015).
13. A. Yazdani, E. H. da Silva Neto, P. Aynajian, Spectroscopic imaging of strongly correlated electronic states. Annu. Rev. Condens. Matter Phys. 7, 11–33 (2016).
14. R. Comin, A. Damascelli, Resonant x-ray scattering studies of charge order in cuprates. Annu. Rev. Condens. Matter Phys. 7, 369–405 (2016).
15. K. Yamada, C. H. Lee, K. Kurahashi, J. Wada, S. Wakimoto, S. Ueki, H. Kimura, Y. Endoh, S. Hosoya, G. Shirane, R. J. Birgeneau, M. Greven, M. A. Kastner, Y. J. Kim, Doping dependence of the spatially modulated dynamical spin correlations and the superconducting-transition temperature in La$_{2-x}$Sr$_x$CuO$_4$. Phys. Rev. B 57, 6165 (1998).
16. S. Blanco-Canosa, A. Frano, E. Schierle, J. Porras, T. Loew, M. Minola, M. Bluschke, E. Weschke, B. Keimer, M. Le Tacon, Resonant x-ray scattering study of charge-density wave correlations in YBa$_2$Cu$_3$O$_{6+x}$. Phys. Rev. B 90, 054513 (2014).
17. M. Hücker, N. B. Christensen, A. T. Holmes, E. Blackburn, E. M. Forgan, R. Liang, D. A. Bonn, W. N. Hardy, O. Gutowski, M. v. Zimmermann, S. M. Hayden, J. Chang, Competing charge, spin, and superconducting orders in underdoped YBa$_2$Cu$_3$O$_y$. Phys. Rev. B 90, 054514 (2014).
18. M. K. Chan, C. J. Dorow, L. Mangin-Thro, Y. Tang, Y. Ge, M. J. Veit, G. Yu, X. Zhao, A. D. Christianson, J. T. Park, Y. Sidis, P. Steffens, D. L. Abernathy, P. Bourges, M. Greven, Commensurate antiferromagnetic excitations as a signature of the pseudogap in the tetragonal high-T_c cuprate HgBa$_2$CuO$_{4+\delta}$. Nat. Commun. 7, 10819 (2016).
19. C. V. Parker, P. Aynajian, E. H. da Silva Neto, A. Pushp, S. Ono, J. Wen, Z. Xu, G. Gu, A. Yazdani, Fluctuating stripes at the onset of the pseudogap in the high-T_c superconductor Bi$_2$Sr$_2$CaCu$_2$O$_{8+x}$. Nature 468, 677 (2010).
20. A. R. Moodenbaugh, Y. Xu, M. Suenaga, T. J. Folkerts, R. N. Shelton, Superconducting properties of La$_{2-x}$Ba$_x$CuO$_4$. Phys. Rev. B 38, 4596 (1988).
21. B. Büchner, M. Breuer, A. Freimuth, A. P. Kampf, Critical buckling for the disappearance of superconductivity in rare-earth-doped La$_{2-x}$Sr$_x$CuO$_4$. Phys. Rev. Lett. 73, 1841–1844 (1994).
22. T. P. Croft, C. Lester, M. S. Senn, A. Bombardi, S. M. Hayden, Charge density wave fluctuations in La$_{2-x}$Sr$_x$CuO$_4$ and their competition with superconductivity. Phys. Rev. B 89, 224513 (2014).

23. N. B. Christensen, J. Chang, J. Larsen, M. Fujita, M. Oda, M. Ido, N. Momono, E. M. Forgan, A. T. Holmes, J. Mesot, M. Huecker, M. v. Zimmermann, Bulk charge stripe order competing with superconductivity in La$_{2-x}$Sr$_x$CuO$_4$ (x=0.12) (2014).

24. J. C. S. Davis, D.-H. Lee, Concepts relating magnetic interactions, intertwined electronic orders, and strongly correlated superconductivity. *Proc. Natl. Acad. Sci. U.S.A.* **110**, 17623–17630 (2013).

25. K. B. Efetov, H. Meier, C. Pépin, Pseudogap state near a quantum critical point. *Nat. Phys.* **9**, 442–446 (2013).

26. S. Sachdev, R. La Placa, Bond order in two-dimensional metals with antiferromagnetic exchange interactions. *Phys. Rev. Lett.* **111**, 027202 (2013).

27. Y. Wang, A. Chubukov, Charge-density-wave order with momentum (2Q,0) and (0,2Q) within the spin-fermion model: Continuous and discrete symmetry breaking, preemptive composite order, and relation to pseudogap in hole-doped cuprates. *Phys. Rev. B* **90**, 035149 (2014).

28. K. Fujita, C. K. Kim, I. Lee, J. Lee, M. H. Hamidian, I. A. Firmo, S. Mukhopadhyay, H. Eisaki, S. Uchida, M. J. Lawler, E.-A. Kim, J. C. Davis, Simultaneous transitions in cuprate momentum-space topology and electronic symmetry breaking. *Science* **344**, 612–616 (2014).

29. See the Supplementary Materials.

30. N. P. Armitage, F. Ronning, D. H. Lu, C. Kim, A. Damascelli, K. M. Shen, D. L. Feng, H. Eisaki, Z.-X. Shen, P. K. Mang, N. Kaneko, M. Greven, Y. Onose, Y. Taguchi, Y. Tokura, Doping dependence of an *n*-type cuprate superconductor investigated by angle-resolved photoemission spectroscopy. *Phys. Rev. Lett.* **88**, 257001 (2002).

31. H. Matsui, T. Takahashi, T. Sato, K. Terashima, H. Ding, T. Uefuji, K. Yamada, Evolution of the pseudogap across the magnet-superconductor phase boundary of Nd$_{2-x}$Ce$_x$CuO$_4$. *Phys. Rev. B* **75**, 224514 (2007).

32. M. d'Astuto, P. K. Mang, P. Giura, A. Shukla, P. Ghigna, A. Mirone, M. Braden, M. Greven, M. Krisch, F. Sette, Anomalous dispersion of longitudinal optical phonons in Nd$_{1.86}$Ce$_{0.14}$CuO$_{4+\delta}$ determined by inelastic x-ray scattering. *Phys. Rev. Lett.* **88**, 167002 (2002).

33. E. M. Motoyama, G. Yu, I. M. Vishik, O. P. Vajk, P. K. Mang, M. Greven, Spin correlations in the electron-doped high-transition-temperature superconductor Nd$_{2-x}$Ce$_x$CuO$_{4\pm\delta}$. *Nature* **445**, 186–189 (2007).

34. V. Thampy, M. P. M. Dean, N. B. Christensen, L. Steinke, Z. Islam, M. Oda, M. Ido, N. Momono, S. B. Wilkins, J. P. Hill, Rotated stripe order and its competition with superconductivity in La$_{1.88}$Sr$_{0.12}$CuO$_4$. *Phys. Rev. B* **90**, 100510 (2014).

35. T. Wu, H. Mayaffre, S. Krämer, M. Horvatic, C. Berthier, W. N. Hardy, R. Liang, D. A. Bonn, M.-H. Julien, Incipient charge order observed by NMR in the normal state of YBa$_2$Cu$_3$O$_y$. *Nat. Commun.* **6**, 6438 (2015).

36. S. Gerber, H. Jang, H. Nojiri, S. Matsuzawa, H. Yasumura, D. A. Bonn, R. Liang, W. N. Hardy, Z. Islam, A. Mehta, S. Song, M. Sikorski, D. Stefanescu, Y. Feng, S. A. Kivelson, T. P. Devereaux, Z.-X. Shen, C.-C. Kao, W.-S. Lee, D. Zhu, J.-S. Lee, Three-dimensional charge density wave order in YBa$_2$Cu$_3$O$_{6.67}$ at high magnetic fields. *Science* **350**, 949–952 (2015).

37. J. Chang, E. Blackburn, O. Ivashko, A. T. Holmes, N. B. Christensen, M. Hücker, R. Liang, D. A. Bonn, W. N. Hardy, U. Rütt, M. v. Zimmermann, E. M. Forgan, S. M. Hayden, Magnetic field controlled charge density wave coupling in underdoped YBa$_2$Cu$_3$O$_{6+x}$. *Nat. Commun.* **7**, 11494 (2016).

38. Y. Hidaka, M. Suzuki, Growth and anisotropic superconducting properties of Nd$_{2-x}$Ce$_x$CuO$_{4-y}$ single crystals. *Nature* **338**, 635–637 (1989).

39. Y. Wang, S. Ono, Y. Onose, G. Gu, Y. Ando, Y. Tokura, S. Uchida, N. P. Ong, Dependence of upper critical field and pairing strength on doping in cuprates. *Science* **299**, 86–89 (2003).

40. P. Abbamonte, E. Demler, J. C. S. Davis, J.-C. Campuzano, Resonant soft X-ray scattering, stripe order, and the electron spectral function in cuprates. *Phys. C Supercond.* **481**, 15–22 (2012).

41. E. G. D. Torre, Y. He, D. Benjamin, E. Demler, Exploring quasiparticles in high-T_c cuprates through photoemission, tunneling, and x-ray scattering experiments. *New J. Phys.* **17**, 022001 (2015).

42. P. K. Mang, S. Larochelle, A. Mehta, O. P. Vajk, A. S. Erickson, L. Lu, W. J. L. Buyers, A. F. Marshall, K. Prokes, M. Greven, Phase decomposition and chemical inhomogeneity in Nd$_{2-x}$Ce$_x$CuO$_{4\pm\delta}$. *Phys. Rev. B* **70**, 094507 (2004).

43. J. P. Hinton, J. D. Koralek, G. Yu, E. M. Motoyama, Y. M. Lu, A. Vishwanath, M. Greven, J. Orenstein, Time-resolved optical reflectivity of the electron-doped Nd$_{2-x}$Ce$_x$CuO$_{4+\delta}$ cuprate superconductor: Evidence for an interplay between competing orders. *Phys. Rev. Lett.* **110** 217002 (2013).

44. H. Saadaoui, Z. Salman, H. Luetkens, T. Prokscha, A. Suter, W. A. MacFarlane, Y. Jiang, K. Jin, R. L. Greene, E. Morenzoni, R. F. Kiefl, The phase diagram of electron-doped La$_{2-x}$Ce$_x$CuO$_{4-\delta}$. *Nat. Commun.* **6**, 6041 (2015).

The following resources related to this article are available online at http://advances.sciencemag.org. (This information is current as of September 14, 2016):

Updated information and services, including high-resolution figures, can be found in the online version of this article at:
http://advances.sciencemag.org/content/2/8/e1600782.full

Supporting Online Material can be found at:
http://advances.sciencemag.org/content/suppl/2016/08/08/2.8.e1600782.DC1

This article **cites 42 articles,** 8 of which you can access for free at:
http://advances.sciencemag.org/content/2/8/e1600782#BIBL